Adsorption of gluconate and uranyl on C-S-H phases: Combination of wet chemistry experiments and molecular dynamics simulations for the binary systems

Iuliia Androniuk, Catherine Landesman, Pierre Henocq, Andrey G. Kalinichev

Adsorption of gluconate and uranyl on C-S-H phases: Combination of wet chemistry experiments and molecular dynamics simulations for the binary systems

Iuliia Androniuk[a], Catherine Landesman[a], Pierre Henocq[b], Andrey G. Kalinichev[a]

a) Subatech, UMR 6447 CNRS/IN2P3, IMT-Atlantique, Université de Nantes, 4 rue Alfred Kastler, 44307 Nantes, France.

b) Andra – French national radioactive waste management agency, 1-7, rue Jean-Monnet, 92298 Châtenay-Malabry cedex, France.

*Corresponding author: C. Landesman, email: Catherine.Landesman@subatech.in2p3.fr

Abstract

As a first step in developing better molecular scale understanding of the effects of organic additives on the adsorption and mobility of radionuclides in cement under conditions of geological nuclear waste repositories, two complementary approaches, wet chemistry experiments and molecular dynamics (MD) computer simulations, were applied to study the sorption behaviour of two simple model systems: gluconate and uranyl on calcium silicate hydrate phases (C-S-H) – the principal mineral component of hardened cement paste (HCP). Experimental data on sorption and desorption kinetics and isotherms of adsorption for gluconate/C-S-H and U(VI)/C-S-H binary systems were collected and quantitatively analysed for C-S-H samples synthesized with various Ca/Si ratios (0.83, 1.0, 1.4) corresponding to various stages of HCP aging and degradation. Gluconate labelled with ^{14}C isotope was used in order to improve the sensitivity of analytical detection technique (LSC) at particularly low concentrations (10^{-8} - 10^{-5} mol/L). There is a noticeable effect of Ca/Si ratio on the gluconate sorption on C-S-H, with stronger sorption at higher Ca/Si ratios. Sorption of organic anions on C-S-H is mediated by the presence of Ca^{2+} at the interface and strongly depends on the surface charge and Ca^{2+} concentration. In parallel, classical MD simulations of the same model systems were performed in order to identify specific surface sorption sites most actively involved in the sorption of gluconate and uranyl on C-S-H and to clarify molecular mechanisms of adsorption.

Key words calcium silicate hydrate, Uranium (VI), gluconate, sorption isotherm, molecular dynamics

1. Introduction

Cementitious materials are expected to be widely used in the design and construction of a geological radioactive waste repository in the argillaceous rock (Callovo-Oxfordian geological formation) in the East of the Parisian basin (e.g., Grambow, 2016). One of the ways to enhance the durability, strength and workability of hardened cement pastes (HCP) is to introduce various types of organic additives into the cement mixture (0.1-2% wt). However, the presence of organic molecules in the HCP pore water can also affect the long-term radionuclide mobility: organic molecules can form water-soluble complexes and compete with radionuclides for sorption sites at the cement surface. Previous studies (Hanehara and Yamada, 1999; Joliecoeur and Simard, 1998; Lesage et al., 2014; Mollah et al., 2000; Nalet and Nonat, 2015; Perez, 2007; Zhu et al., 2014) were mostly focused on the effect of additives on the hydration processes, while much less efforts were made (e. g. Glaus et al., 2006; Pointeau et al., 2008) to understand and explain their postproduction effects within the contest of radioactive waste storage applications. The development of a quantitative molecular scale understanding of these effects, based on a simplified model system, is the primary objective of this work.

Cement is mostly composed of calcium silicates, aluminates and aluminoferrites. The main hydration product of cement (up to 70% of the total mass) and its principal binding component are calcium silicate hydrate (C-S-H) phases. They are formed by the interaction of alite (C_3S) and belite (C_2S) with water. Being the most essential part, C-S-H phase was selected as a model of a typical cement system. Uranium (VI) was selected as a model radionuclide because it is one of the most important and well-studied actinide elements that strongly sorbs on C-S-H in the form of the uranyl ion UO_2^{2+}. The chemical mechanisms of its sorption processes on C-S-H phases have been previously studied by Pointeau et al., 2004; Harfouche et al., 2006; Tits et al., 2011; Gaona et al., 2012; Mace et al., 2013. Gluconate (anionic form of the gluconic acid, $C_6H_{12}O_7$) was used in our work as a model organic additive because it is a simple organic molecule with well-described structure, chemically stable in highly alkaline solutions, and a strong complexing agent towards cations. It is also important that gluconate has the same functional groups as more complex polycarboxylic polymers that are used as actual superplasticisers in cement production. Earlier studies of the binary systems (C-S-H/gluconate, HCP/gluconate (Glaus et al., 2006) and C-S-H/U(VI) (Pointeau et al., 2004; Tits et al., 2011)) provide initial reference data for the investigation of a more complex ternary system (C-S-H/gluconate/U(VI)).

Cementitious materials are truly multiscale and their molecular level properties can be difficult to understand and interpret without having in mind a clear atomistic picture of the structure and processes involved. Computational molecular modelling is very helpful in this respect by allowing a consistent interpretation of the observed interfacial behaviour on the fundamental molecular scale considering the effects of local C-S-H surface structure and composition on the interaction (Kalinichev et al., 2007; Sanchez and Sobolev, 2010). Our study is designed to get understanding of the molecular mechanisms of such interactions using a combination of several experimental techniques and computational molecular modelling approaches.

2. Materials and methods

2.1. Synthesis and characterization of C-S-H

Synthetic C-S-H phases were prepared individually in PPCO centrifuge tubes (Nalgene™) by the direct reaction of calcium oxide (Sigma Aldrich, ≥ 99.9%) and silica fume (Aerosil® 200, Evonik) in degasified water with solid-to-water ratios of 2×10^{-2} kg/L. This method allows obtaining C-S-H gels with different Ca/Si ratios by controlling the amount of initial reagents.

Degasified water was prepared by heating (T=50°C) and steering under partial vacuum of Milli-Q® ultrapure water (>18.2 MΩ·cm). The synthesis was performed in the absence of carbon dioxide in a glove-box under inert atmosphere (argon). Three compositions of calcium silicate hydrates were synthesised corresponding to three values of Ca/Si ratio (0.83, 1.0 and 1.4) in order to be able to compare the sorption properties of pure hydrate phases.

After an aging period of 1 month, the suspensions were centrifuged (4000 rpm, 40 min) and filtered through 0.22 µm PTFE syringe membrane filters (VWR). Separated solids were analysed by XRD (D5000, Bruker) to confirm the absence of crystalline phases such as portlandite (excess of calcium) and calcite (carbonation). Before the analysis, solids were dried in inert atmosphere over silica gel for 2 weeks. The resulting diffractograms were compared with the reference patterns from the ICDD-PDF database. No peaks of portlandite and calcium carbonate polymorphs were detected. Thus, the phases were assumed to be “pure” (single-phase). pH values were measured using a combined microelectrode (Radiometer) calibrated with buffer solutions of 9.18 (pH9.180, Radiometer Analytical) and 12.45 pH (pH12.45, Radiometer Analytical) at room temperature (T = 23°C). Concentrations of Si and Ca in solutions were measured by quadrupole inductively coupled plasma - mass spectrometry (XSeries II ICP-MS, Thermo Fisher Scientific) and cation-exchange ion

chromatography (ICS1000, Thermo Scientific Dionex). The resulting Ca/Si ratios were calculated from the difference between the initial and residual (after equilibration) amounts of Ca and Si (see Table 1). It was confirmed that the synthesised C-S-H phases had the Ca/Si ratios that corresponded to the target ones and their equilibrium characteristics agree well with literature data (Chen et al., 2004; Lothenbach and Nonat, 2015).

Table 1. Characterisation of C-S-H equilibrated solutions.

Ca/Si ratio (target)	pH value	[Si] equilibrated in solution, mol/L	[Ca] equilibrated in solution, mol/L	Ca/Si ratio (calculated)
0.83	10.24±0.05	$(2.68\pm0.31)\times10^{-3}$	$(1.25\pm0.12)\times10^{-3}$	0.85±0.05
1.0	11.51±0.05	$(0.42\pm0.63)\times10^{-4}$	$(2.10\pm0.12)\times10^{-3}$	0.98±0.05
1.4	12.32±0.05	$(1.70\pm0.71)\times10^{-5}$	$(11.10\pm0.12)\times10^{-3}$	1.38±0.05

2.2. Wet chemistry experiments

Sorption process is classically described by an adsorption isotherm (concentration of ion sorbed as a function of ion concentration in equilibrated solution). Series of batch experiments were performed to evaluate the sorption of gluconate (D-Gluconic acid sodium salt, ≥ 99%, Sigma Aldrich) and ^{238}U (VI) on C-S-H with various Ca/Si ratios by using the method of depletion in solution (eqs. 1 and 2). The solutions were separated by centrifugation (4000 rpm, 40 min) and filtered through 0.22 µm PTFE syringe membrane filters (VWR). The amount of C-S-H was estimated from the amount of Si in the solid (eq. 3):

$$[\text{Gluconate}]_{\text{sorbed}} = ([\text{Gluconate}]_{\text{initial}} - [\text{Gluconate}]_{\text{solution}}) \times (V/Q(\text{Si})_{\text{C-S-H}}) \quad (1)$$

$$[\text{U(VI)}]_{\text{sorbed}} = ([\text{U(VI)}]_{\text{initial}} - [\text{U(VI)}]_{\text{solution}}) \times (V/Q(\text{Si})_{\text{C-S-H}}) \quad (2)$$

$$Q(\text{Si})_{\text{C-S-H}} = Q(\text{Si})_{\text{initial}} - Q(\text{Si})_{\text{solution}} \quad (3)$$

where $[\text{species}]_{\text{sorbed}}$ is the concentration on the solid (mmol/mol of Si); $[\text{species}]_{\text{initial}}$ is the concentration initially present in solution (mmol/L); $[\text{species}]_{\text{aolution}}$ is the equilibrium concentration in solution (mmol/L); V is the

solution volume (L); $Q(Si)_{C\text{-}S\text{-}H}$ is the amount of Si in C-S-H (mol); $Q(Si)_{initial}$ is the concentration of Si initially added during synthesis (mol); $Q(Si)_{solution}$ is the equilibrium concentration of Si in solution.

Sorption can be characterised by the distribution ratio (*R*d), describing the distribution of the species of interest (here gluconate and U(VI)) between the solid phase and the liquid phase in a batch sorption experiment:

$$R\text{d (L/kg}_{solid}) = ([\text{Gluconate}]_{sorbed} / [\text{Gluconate}]_{solution}) \times L/S \quad (4)$$

where *L*/*S* is the liquid to solid ratio (L/kg). For the *L*/*S* calculation the amount of solid was estimated after drying the C-S-H samples at T = 60°C for 48 hours.

For sorption experiments initial gluconate concentrations were ranging from 10^{-5} to 10^{-2} mol/L. Non-radioactive (stable) gluconate was analysed by DIONEX ICS-1000 ion chromatography system (IonPac AS18 hydroxide-selective anion-exchange column coupled with a conductivity detector). The eluent consisted of a 5mM KOH solution at a flow rate of 1 ml/min. Gluconate standard solutions (D-Gluconic acid sodium salt, ≥ 99%, Sigma Aldrich) were used for the calibration curve in the range from 0.5 to 10 mg/L. An injection loop of 100 µl was used to lower the detection limit for gluconate (0.5 mg/L of gluconate).

The kinetics of adsorption was studied by measuring the evolution of gluconate concentration in contact solution after 0.5, 1, 3, 7, 15 and 30 days of reaction (for the initial gluconate concentration of 1.03×10^{-3} mol/L). For all samples, a full ion analysis with IC was performed to provide a complete system description. Sodium concentrations were also analysed because Na^+ was added to the systems as a counterion of gluconate.

For low concentrations, ranging from 10^{-9} to 10^{-6} mol/L, mixtures of stable and ^{14}C radiolabelled gluconate (D-[1-^{14}C], > 99%, ARC) were used. Equilibrated solutions were then analysed by liquid scintillation counting (Tri-Carb 3170 TR/SL, PerkinElmer) in order to determine the residual amount of the radioactive tracer. When radiotracers were used, the amount of adsorption was calculated using equation (1) with the activity of ^{14}C-gluconate instead of the concentration, assuming full isotopic exchange between ^{14}C labelled and stable gluconate.

The solids separated by centrifugation at the end of the sorption experiment were used for the desorption studies (kinetics and isotherms). 25 ml of organics-free solutions prepared with the pH and concentrations of Ca

and Si defined by the C-S-H steady state (Table 1) were then added to the samples. The gluconate concentration at the end of the desorption step was then calculated as:

$$[\text{Gluconate}]_{\text{desorption}} = [\text{Gluconate}]_{\text{sorbed}} - [\text{Gluconate}]_{\text{desorbed}} \quad (5)$$

where $[\text{Gluconate}]_{\text{desorption}}$ is the gluconate concentration on the solid at the end of the desorption step (mmol/mol of Si); $[\text{Gluconate}]_{\text{sorbed}}$ is the gluconate concentration on the solid at the end of the adsorption step (mmol/mol of Si); $[\text{Gluconate}]_{\text{desorbed}}$ is the equilibrium gluconate concentration in solution at the end of the desorption step (mmol/mol of Si). For the calculation of $[\text{Gluconate}]_{\text{desorbed}}$, the amount of gluconate in the residual solution left after solid separation was evaluated. The water content for each C-S-H phase was calculated by weight loss during drying at 60°C.

U(VI) sorption experiments were performed on C-S-H with Ca/Si = 1.4. The initial concentrations were ranging from 10^{-5} to 10^{-2} mol/L. For each concentration, an appropriate volume of ^{238}U solution in 10^{-2} mol/L hydrochloric acid was added to the C-S-H suspension. A contact time of 2 weeks was applied. The range of concentrations was selected to avoid the formation of U(VI) precipitates ([U] < 10^{-2} mol/L) (Tits et al, 2011). U(VI) concentrations were measured by ICP-MS using the standard solution for the external calibration curve (ICP Standard, ^{238}U, SCP Science; in the range from 0.005 to 0.5 μg/L). A full ion analysis was also performed.

For both studies (U(VI) and gluconate), the uncertainties of each experimental step were calculated (micropipettes, scales, ICP-MS, IC, LSC, etc.) and the quadratic propagation formula was applied under an assumption of independent variables (Ku, 1966). The results were then expressed at an uncertainty level of 95% (k = 2).

2.3. Computational methods

The atomistic description of highly disordered C-S-H phases is much more challenging than a description of crystalline phases. However, numerous experimental studies (neutron scattering (Allen, 2007), ^{43}Ca NMR (Bowers and Kirkpatrick, 2009), ^{29}Si NMR (Brunet et al., 2004), XRD, TEM, EXAFS (Grangeon et al., 2013)) suggested that the crystal structure of tobermorite is one of the closest to the real cement hydrate. The unit cell parameters and atomic coordinates of tobermorite-11 Å (Hamid, 1981) were used as the basis of our atomistic C-S-H models. The simulations supercell was then formed by the unit cell multiplication along x and y dimensions. The bulk tobermorite supercell of 6 × 6 × 1 (40.2 × 44.4 × 25.5 Å^3) was cleaved in the middle of

interlayer along the (0 0 1) crystallographic plane – the typical cleavage plane for this layered crystal – to create a basic model of the C-S-H surface which was then further modified to construct models of C-S-H surfaces with various Ca/Si ratios. Since the surface is the primary object of interest in our study, it was decided that only the composition of the top layers of the cleaved crystal (those in direct contact with the model solutions) would be modified to produce the required Ca/Si ratios, leaving the initial stoichiometric tobermorite in the middle of the model structure.

The model C-S-H surfaces corresponding to different Ca/Si ratios can be constructed in two ways: 1) by randomly removing silica tetrahedra from the crystalline tobermorite structure using as a guidance the ^{29}Si MAS NMR data for C-S-H (Cong and Kirkpatrick, 1996; Beaudoin et al., 2009); 2) by introducing additional Ca^{2+} cations into the interlayer. To achieve higher Ca/Si ratios, the bridging tetrahedra were extracted randomly taking into account that a dimer is the most abundant of all silicate species in C-S-H and a linear pentamer is the second most abundant (Richardson et al., 2010; Sáez del Bosque et al., 2016). For each model surface the amount of added Ca^{2+} was different, reflecting the required Ca/Si ratio. The formation of defects in the silicate chains can result in extra adsorption of water molecules at the surface. At the same time, H_2O dissociation in reactive media leads to the formation of additional hydroxyl groups on the surface and protons that bind at the sites of missing silicon tetrahedra. Different cases of protonation (Churakov et al., 2014) should be considered since they can result in the accumulation of different surface charge. Aqueous hydroxyl ions were added to the system in order to maintain the total electrostatic neutrality of the models. For the C-S-H model with the lowest Ca/Si ratio all silanol groups of bridging Si and one of the pairing Si (replacing the introduced defect) were deprotonated; for the C-S-H models with high Ca/Si ratio all of the surface silanol groups were deprotonated. The deprotonated oxygens of the surface were assigned a higher partial charge (q = -1.3|e|) than the protonated ones, following the atomistic models of kanemite (Kirkpatrick et al., 2005). Three dimensional periodic boundary conditions were applied to the constructed model interfaces, and for each Ca/Si ratio three such interfaces were simulated: C-S-H/water, C-S-H/uranyl solution, and C-S-H/gluconate solution.

Most interatomic interaction parameters, including the partial atomic charges for C-S-H, H_2O, and Ca^{2+} ions were taken from the ClayFF parameterization (Cygan et al., 2004) and its later modifications for cement systems (Kirkpatrick et al., 2005; Kalinichev et al., 2007). The interaction parameters for uranyl ions used in this work (Guilbaud and Wipff, 1993, 1996) are also consistent with ClayFF (Teich-McGoldrick et al., 2014). For

organic gluconate the GAFF set of parameters was used (Wang et al., 2004). Standard Lorenz-Berthelot mixing rules were applied to calculate short-range Lennard-Jones interactions between the unlike atoms. Long-range electrostatic forces were evaluated by means of the Ewald summation method. Materials Studio software package (BIOVIA, San Diego, CA, USA) was used to prepare the simulation models and to visualize the results, but all simulations were carried out with the LAMMPS software package (Plimpton, 1995).

Geometry optimisation of each model structure was performed first using the Polak-Ribiere version of the conjugate gradient algorithm of energy minimization. The optimized structures were then used in molecular dynamics (MD) simulations. The Verlet leapfrog algorithm was used to integrate the equations of motion with a time step of 0.001 ps. During the pre-equilibration MD run performed for each model system, several parameters were carefully monitored: individual components of the potential energy, density, stabilization of the system atomic configuration. After an equilibration period of ~1 ns (*NPT*-ensemble), the main MD production runs for each system were performed for 2 ns (*NVT*-ensemble). Ambient conditions (T = 300 K, P = 0.1 MPa) were assumed in all MD runs.

3. Results and discussion

3.1. Adsorption experiments

3.1.1. U(VI) – C-S-H system

The behaviour of the binary C-S-H/U(VI) system was investigated for the C-S-H sample with the highest Ca/Si ratio of 1.4. It is thought that U(VI) binding by C-S-H is mostly happening due to the surface sorption and might involve Ca uptake. Sorption is the highest under alkali-free conditions and it was found to be dependent on pH and the C-S-H composition (Tits et al., 2011).

The presently obtained results for isothermal adsorption (Fig. 1) show the approximately linear behaviour: the slope of ~1, with the coefficient of determination of R^2 = 0.98. This is in good agreement with the data reported earlier by Tits et al. (2011) for C-S-H with Ca/Si ratios of 0.75 and 1.07. In their work the non-linear behaviour was observed for C-S-H phase with Ca/Si = 1.65 and at higher pH = 13.3, when the formation of aqueous hydroxo complexes in solution of U(VI) ($UO_2(OH)_4^{2-}$) becomes preferable to the sorption. It still remains unclear at what Ca/Si ratio this transition actually occurs. The results of our work provide additional information on the

U(VI) interaction with C-S-H in the range of intermediate Ca/Si ratios between 1.07 and 1.65 discussed above. From our results, the adsorption isotherm at pH = 12.3 is already slightly non-linear but this non-linearity is not yet well-defined, so the sorption of U(VI) remains the dominant process.

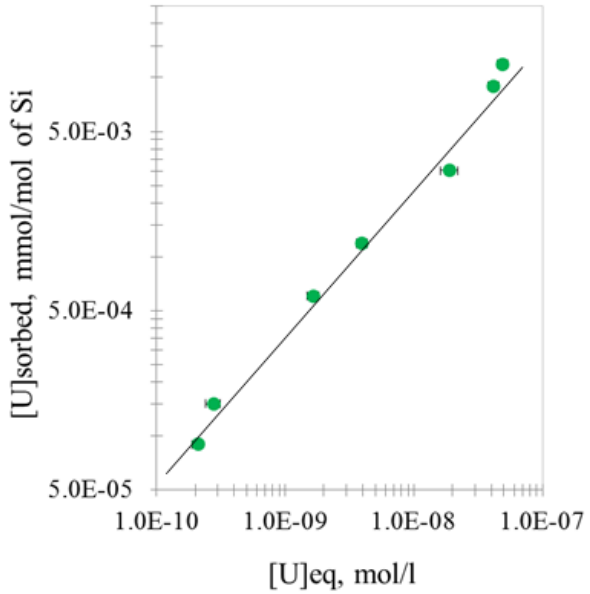

Fig. 1. The isotherm of U(VI) adsorption on C-S-H with Ca/Si = 1.4, *S*/*L* = 20 g/L.

The evolutions of pH, Ca and Si concentrations were measured and presented in Table 2. No changes in pH and Si concentrations were observed. As reported by Tits et al. (2011), the addition of U(VI) does not greatly affect the equilibrium state of C-S-H phases. Three main sorption species were identified by Tits et al. (2015): a surface complex, incorporated species, and a surface precipitate. A slight increase in Ca concentration with the increase of U(VI) initial concentration may be caused by Ca-U(VI) exchange on the sorption sites of the C-S-H surface.

Table 2. pH, Si and Ca concentrations in C-S-H equilibrated solution as a function of U(VI) concentration in equilibrium (C-S-H with Ca/Si = 1.4).

[U] in equilibrium, mmol/L	pH values	[Ca] in equilibrium, mmol/L	[Si] in equilibrium, mmol/L
$(2.10\pm0.11)\times10^{-7}$	12.35±0.05	8.93±0.73	0.028±0.0.002

$(2.71\pm0.14)\times10^{-7}$	12.29±0.05	7.72±0.64	0.030±0.0.002
$(1.63\pm0.08)\times10^{-6}$	12.25±0.05	8.09±0.67	0.029±0.0.002
$(3.90\pm0.19)\times10^{-6}$	12.36±0.05	8.48±0.69	0.029±0.0.002
$(1.92\pm0.09)\times10^{-5}$	12.23±0.05	11.03±0.87	0.028±0.0.002
$(4.21\pm0.20)\times10^{-5}$	12.31±0.05	11.15±0.89	0.031±0.0.002
$(4.91\pm0.25)\times10^{-5}$	12.35±0.05	12.07±0.96	0.030±0.0.002

3.1.2. Gluconate – C-S-H systems

The kinetics of gluconate adsorption on C-S-H was investigated for all C-S-H phases with different Ca/Si ratios. The adsorption of gluconate was relatively fast, with the reactions almost completed within 1 day and reaching a steady state in 3 days (Fig. 2). Thus, a contact time of 3 days for adsorption isotherm studies was selected. Rapid sorption was also observed for hydrated cement paste as reported by Glaus et al. (2006). Fast kinetics is generally interpreted as evidence of the predominance of surface sorption processes over incorporation into the structure.

Figure 2 (right) presents combined results of two sorption experiments performed for ^{14}C-labelled gluconate (10^{-9} to 10^{-5} mol/L) and stable-C gluconate (10^{-5} to 10^{-2} mol/L). The sorption isotherms show the influence of Ca/Si ratio on the gluconate adsorption by C-S-H phases. For the three C-S-H compositions studied, the sorption gradually increases for the entire concentration range used, with higher sorption at lower Ca/Si ratios. The data overlap between the two analytical methods used (ion chromatography and liquid scintillation counting) demonstrates good reproducibility of the results.

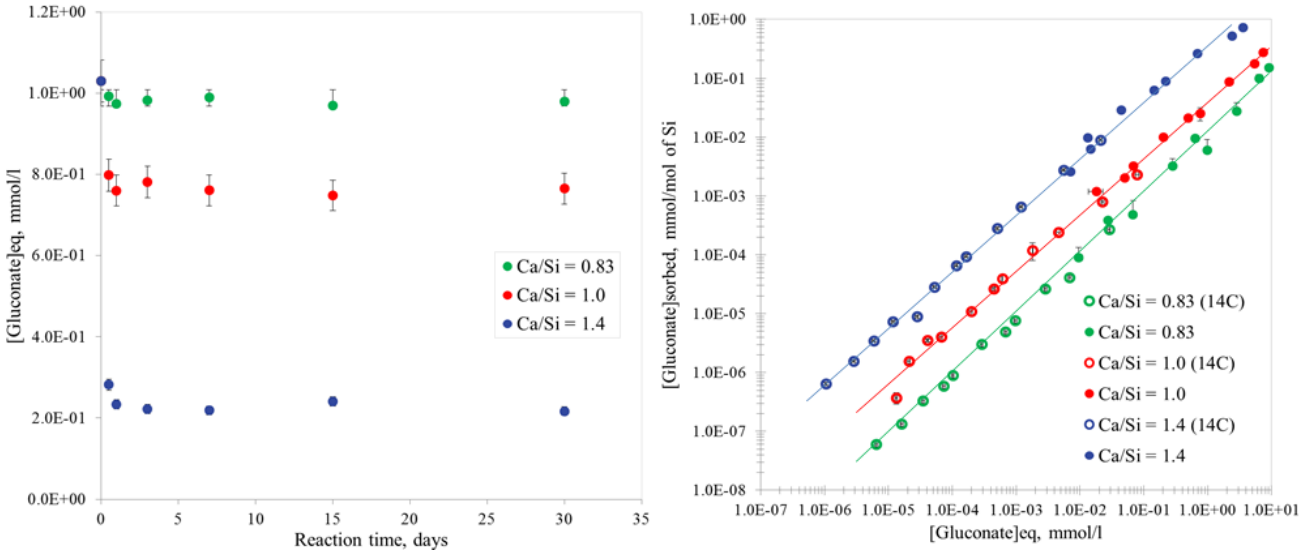

Fig. 2. Kinetics of gluconate adsorption on C-S-H (left) and isotherms of gluconate adsorption (right) for C-S-H phases with 3 Ca/Si ratios (0.83, 1.0, 1.4), *S*/*L* = 20 g/L.

The calculated distribution coefficients (R_d) have the maximum values of approximately 285, 40, and 4.5 L/kg for the C-S-H samples with Ca/Si = 1.4, 1.0, and 0.83, respectively. The sorption at small concentrations ($[Gluconate]_{eq} < 10^{-3}$ mol/L) is approximately linear for all C-S-H compositions studied leading to a nearly constant *R*d value. The linear sorption (the slope of the isotherm ≈ 1) may be an indication of the presence of one type of the preferential sorption site or of several sites with equal probabilities of the adsorbate binding.

The gradual increase in the amount of gluconate sorbed on C-S-H can be explained by electrostatic interactions between the surface and the adsorbate. It is known that with increasing Ca/Si ratio the net surface charge changes from negative to positive as a result of Ca^{2+} overcharging (Viallis-Terrisse et al., 2001). In alkaline solutions gluconate exists in the form of a negatively charged ion (pK_a of gluconate carboxyl group is 3.86), so its adsorption would be driven primarily by electrostatic forces. At the same time, the hydroxyl groups of gluconate are expected to remain protonated in the given pH range (pK_a of the most acidic hydroxyl group is approximately 13, according to Zhang et al., 2007)). The observed rapid kinetics of adsorption (steady state reached after only 1 day) is also in agreement with this assumption.

For a complete description of the studied systems, full cation and anion analysis was performed for each sample: pH, [Ca], [Si], [Gluconate], [Na]. The results for major cations are presented in Fig. 3.

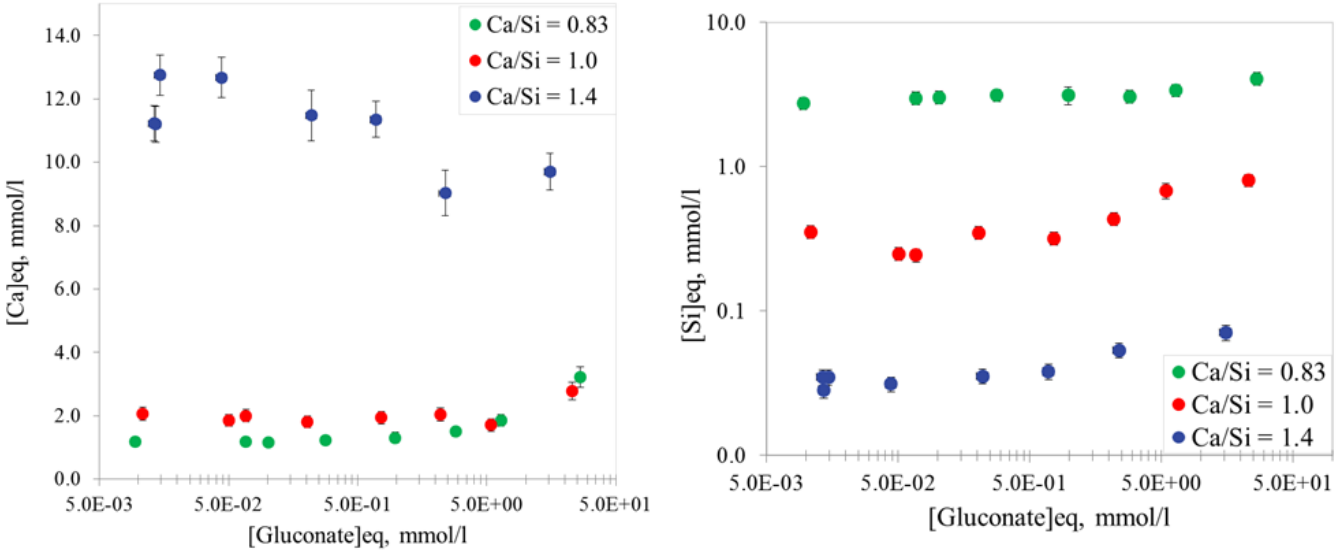

Fig. 3. Evolution of Si (left) and Ca (right) concentrations in the C-S-H equilibrated solution as a function of gluconate concentration at the steady state.

Sodium was added to the system as a counterion of gluconate (sodium salt of gluconic acid). It was found that the addition of Na^+ in relatively small concentrations (the same concentration range as for the gluconate ion) does not affect the equilibrium state of C-S-H. Nalet and Nonat (2016) reported results for the adsorption of gluconate on C-S-H for higher concentrations. In their case, the presence of gluconate can seriously change concentrations of major cations in the equilibrium state since it is a strong complexing agent for Ca. But for $[Gluconate]_{eq}$ < 5 mmol/L, Ca and Si concentrations are not affected significantly. No change in pH values was also observed for all C-S-H phases. This means that the presence of gluconate at low concentrations does not cause measurable transformations of the C-S-H phases.

The results of the present study can be compared with the gluconate sorption measurements on hydrated cement paste (Glaus et al., 2006) taking into account that for HCP the Ca/Si ratio is higher (circa 1.6) and that C-S-H phases represent a mass fraction of about 70%. According to the presented trend for C-S-H phases, more gluconate should be sorbed on the hydrated cement phase. The estimated *R*d values for HCP (Glaus et al., 2006) are 100 times higher (>10^4 L/kg) than for C-S-H with Ca/Si = 1.4. It can be suggested that C-S-H can be considered as the main phase responsible for the adsorption of organic anions from solution but it is clearly not the only one.

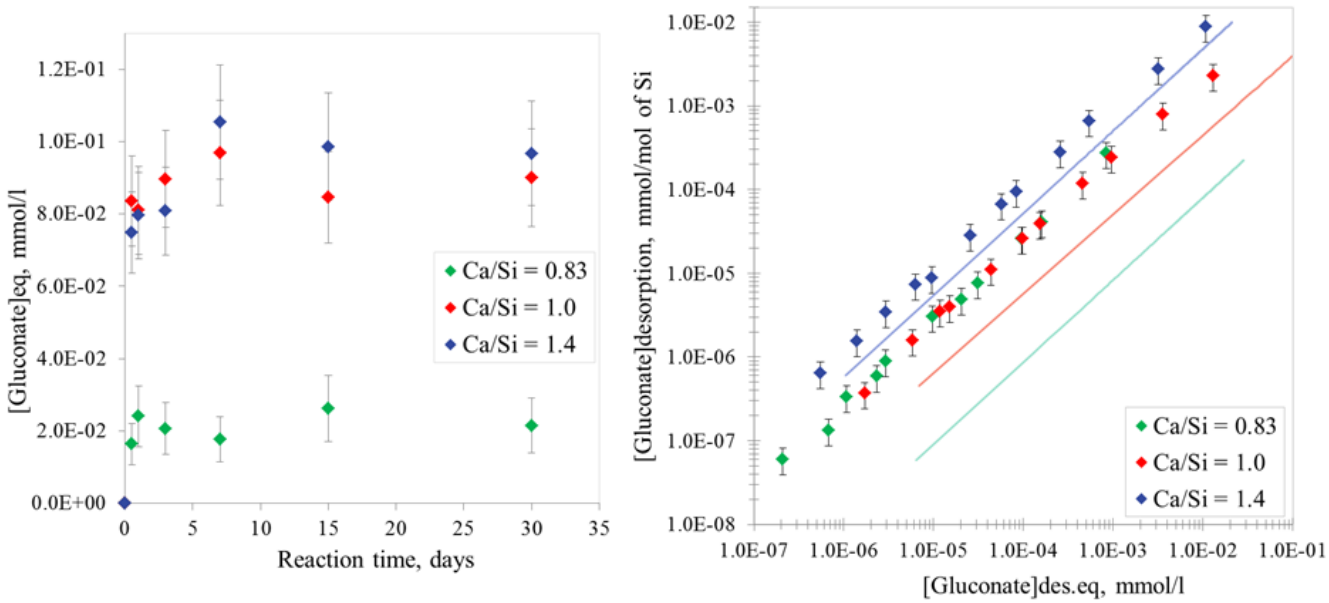

Fig. 4. Kinetics of gluconate desorption from C-S-H (left) and isotherms of gluconate desorption (right) from the C-S-H phases with 3 Ca/Si ratios (0.83, 1.0, 1.4), *S*/*L* = 20 g/L. Lines show averaged positions of the sorption isotherms.

The desorption kinetics and isotherms of gluconate from C-S-H are reported in Fig. 4. All systems reached a steady state in 1 day, so the reaction time of 3 days was selected for the desorption study. It was observed that the desorption is not fully reversible for all C-S-H phases studied indicating the occurrence of additional chemical processes. It can be seen that the hysteresis is more prominent for the C-S-H composition with lower Ca/Si ratio, while the sorption is reversible for Ca/Si = 1.4 within the stated levels of uncertainty for both experiments. The observed desorption hysteresis can also be a result of the sorption non-equilibrium.

To our knowledge, the desorption processes of gluconate on C-S-H have never been studied before, and only a comparison with the data for hydrated cement paste (Glaus et al., 2006) is then possible. In that work, two sorption sites for gluconate where classically defined: a strong site and a weak site. The sorption process was found to be reversible for the weak site and the reversibility of the strong site was assumed based on the experimental results for α-isosaccharinic acid (α-ISA) desorption. However, the nature of the weak and the strong sites remained undefined. The C-S-H surface provides different sorption sites for organic anion that have to be studied (see the molecular modelling section below). Also, some of the hydroxyl groups of gluconate may

participate in the sorption process and contribute to its stronger binding on the C-S-H surface. The calculated uncertainties are large due to the propagation through numerous steps of the desorption experiment. Wet chemistry experiments allow identification of the main trends in the behaviour of the investigated species on C-S-H surfaces, but they do not provide sufficient information on the molecular mechanisms involved. Thus, molecular modelling was further used here as a tool for the interpretation of macroscopic observations.

3.2. Molecular modelling of binary systems

The structure and composition of MD-simulated C-S-H-solution interfaces was quantitatively analysed in the form of atomic density profiles (Fig. 5). These profiles, as well as other simulated properties, were calculated as time averages over the entire duration of the corresponding equilibrium production runs and over two statistically independent solid/solution interfaces created after the C-S-H crystal cleavage for each simulation box: both surfaces are characterized by the same amount of created structural defects and are in contact with the solution of the same composition. The thickness of the aqueous layer separating two surfaces was large enough (≈ 70 Å) to ensure that the interactions at the one surface would not affect the other and result in bulk-like behaviour of the model solution in the middle of the aqueous layer simulation box. The distance of solution atoms from the surface, *d*, was calculated taking as a reference (*d* = 0) the average *z*-coordinates of the oxygen atoms of the top-most pairing Si tetrahedra at each C-S-H surface.

3.2.1. Uranium (VI) – C-S-H system

In alkaline solutions U(VI) exists in the form of uranyl cation UO_2^{2+}. In aqueous environment uranyl ion is usually coordinated in the first hydration shell by 5 H_2O molecules (Guilbaud and Wipff, 1993,1996) some of which can be substituted by hydroxyl ions at high pH. Although the number of uranyl ions introduced to the system was limited to 8, some adsorbed aqua complexes were observed on the C-S-H surface.

The calculated atomic density profiles reveal clear differences in the uranyl/C-S-H interaction at two Ca/Si ratios. Formation of two types of complexes can be seen for Ca/Si = 0.83 (Fig. 5 (left)) with UO_2^{2+} peaks located, respectively, around 3-4 Å (inner-sphere surface complex) and at 5-6 Å (outer-sphere surface complex).

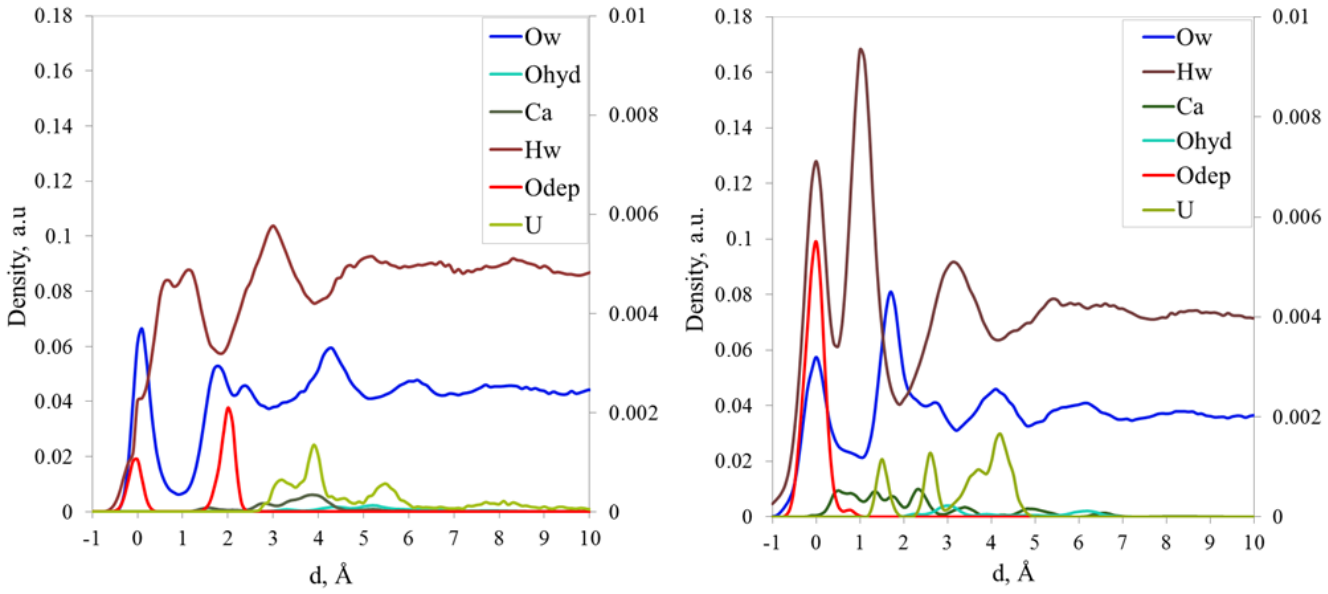

Fig. 5. Atomic density profiles of UO_2^{2+} containing solutions near C-S-H surfaces: left – Ca/Si = 0.83; right – Ca/Si = 1.4. The profiles of U are shown with an enlarged auxiliary scale on the right for clarity. Abbreviations: Ow and Hw – O and H of water; Ohyd – O of solution hydroxyl group; Odep – deprotonated silanol group of the surface.

All adsorbed uranyl ions remain in the five-fold coordination with oxygens in the equatorial plane. Previous studies have shown that the linear $[O=U=O]^{2+}$ structure is preserved upon sorption onto C-S-H or incorporation in the C-S-H structure (Harfouche et al., 2006; Mace et al., 2013; Tits et al., 2011). Furthermore, the inner-sphere coordination of UO_2^{2+} appears to be the predominant type of interaction with the surface (Fig. 6(a)). Fig. 6 also demonstrates that uranyl complexation with the surface groups of pairing silicon tetrahedra is blocked by the presence of two axial oxygen atoms and considerable number of bridging tetrahedra on the C-S-H surface at the lowest Ca/Si ratio.

Outer-sphere surface complexes are mostly coordinated by two deprotonated hydroxyls of the bridging Si tetrahedra (as it is shown on a typical simulation snapshot in Fig. 6(b).The positions of both complexes can be easily identified looking at the atomic density surface maps calculated for the defined interfacial solution layers (see Fig. 5).

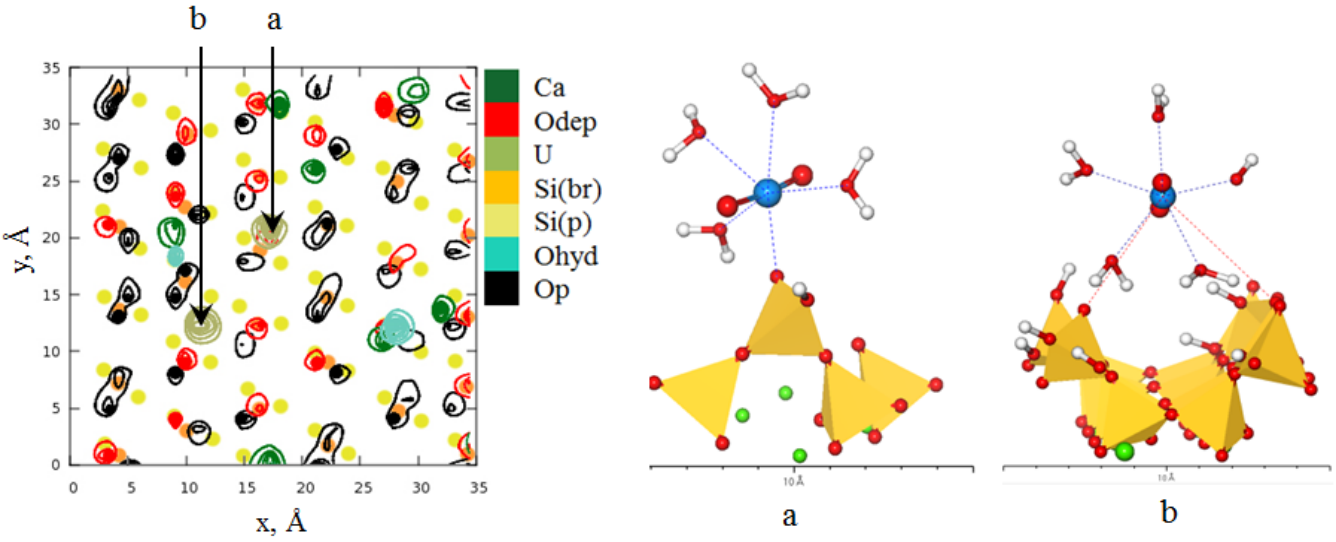

Fig. 6. Left: time-averaged atomic density surface maps of UO_2^{2+} ions within 2.5 – 4.5 Å from the C-S-H surface (the first molecular layer) at Ca/Si = 0.83. Right: typical coordination of the inner-sphere (a) and outer-sphere (b) UO_2^{2+} surface complexes. Colour scheme: yellow – Si, red – O, white – H, blue – U.

When the surface contains only Si dimers (Ca/Si = 1.4) a new sorption site can be identified. In this case the atomic density profile of uranium distribution (Fig. 5 (right)) near the surface reveals three distinct peaks. The peak positions are shifted closer the surface since all bridging Si tetrahedra are absent from the C-S-H model studied. The first peak (~1-2 Å) corresponds to the uranyl cations complexing with two deprotonated silanol groups of the surface in their coordination sphere (bidentate coordination, see Fig. 7 below). Monodentate inner-sphere surface complexation of uranyl is evidenced by the second peak of uranyl distribution at ~2-3 Å from the surface. Similar to other interfaces, the uranyl cations located more than 3 Å from the surface are assumed to be forming outer-sphere complexes and preserve their hydration shell almost unperturbed. Since all bridging silicon tetrahedra are missing at this high Ca/Si ratio, it is much easier for the uranyl cation to reach the deprotonated sites of the paring tetrahedra and form stronger inner-sphere complexes.

In general, UO_2^{2+} cations are bound to the same surface sites as Ca^{2+} cations and a competition between them can be expected. There is also a preferential UO_2^{2+} coordination to the deprotonated sorption sites (more negatively charged). When the surface silanol groups are all deprotonated under high pH conditions, the bidentate adsorption configuration is strongly predominant to the monodentate configuration.

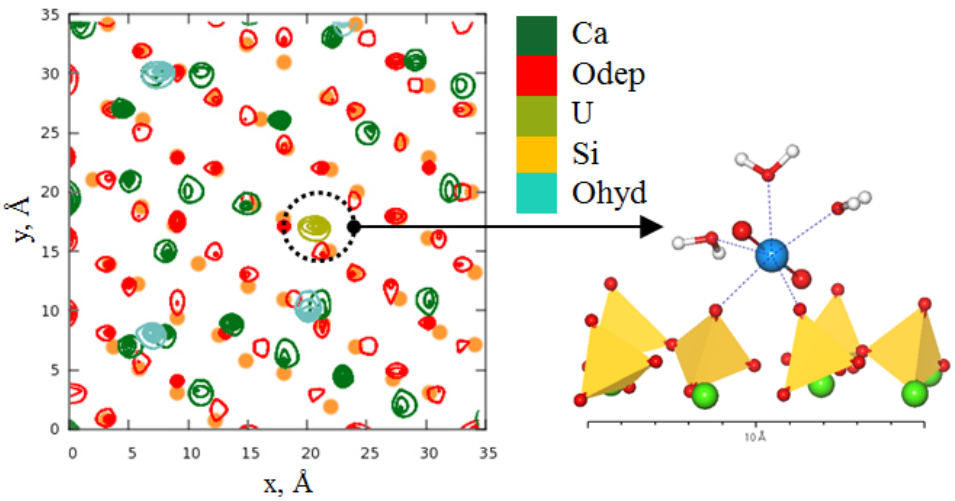

Fig. 7. Inner-sphere complex of uranyl ion with CSH surface at Ca/Si = 1.4: left - distribution of aqueous species within 1–2 Å from the C-S-H surface (the first molecular layer of surface solution); right – a typical simulation snapshot illustrating the inner-sphere bidentate configuration.

3.2.2. Gluconate – C-S-H system

The adsorption behaviour of the organic anions was also evaluated using the same C-S-H – solution models. The simulated molecular structure of the adsorption layers at the liquid-solid interface are illustrated in Fig. 8. When the gluconate concentration in solution is relatively low, its molecules will mostly attach to the surface through the most active functional group – the deprotonated carboxyl group (single-group adsorption, Fig. 8). The hydroxyl groups of gluconate do not contribute to complexation. Negatively charged gluconate cannot form inner-sphere complexes directly with the C-S-H surface, which is also nominally negatively charged. However, as the analysis of C-S-H/gluconate interface shows, it can create complexes with Ca^{2+} ions present on the surface (cation bridging complexation). This cation bridging can be clearly identified from the calculated atomic density profiles of various species at the interface (Fig. 8): Ca^{2+} at distances of ~0.5-1.5 Å forms inner-sphere complexes with deprotonated surface sites (defined as d = 0 Å) and is further coordinated by carboxyl groups of gluconate (the peak of Ocarb at ~2.5-3.5 Å).

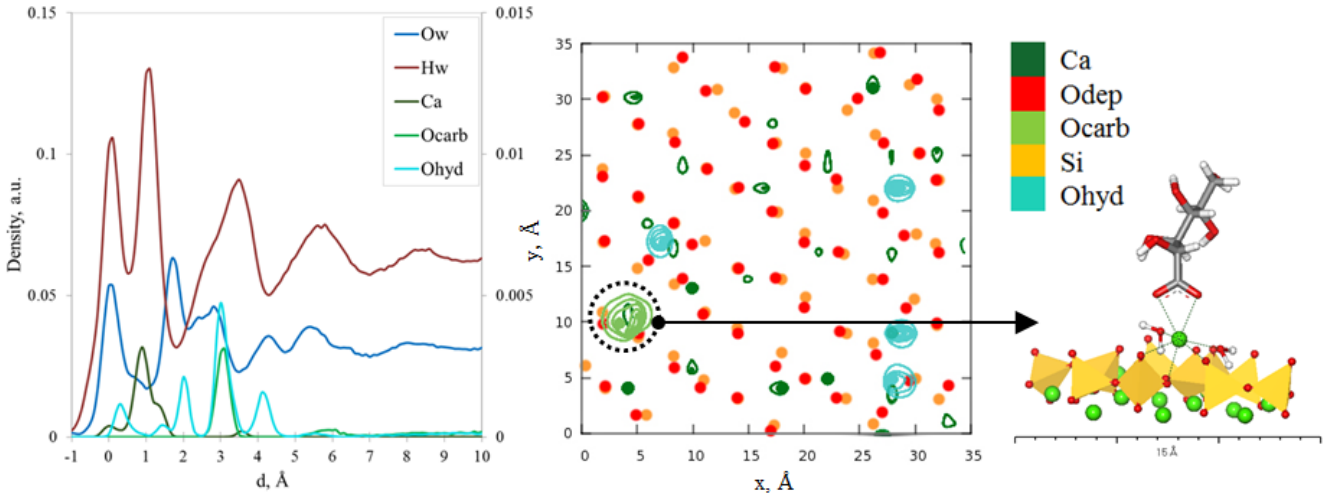

Fig. 8. Atomic density profiles near C-S-H surface (Ca/Si = 1.4) for the solution containing gluconate (left), surface distribution of ions (middle), and a snapshot illustrating the cation bridging surface complexation. Ocarb – oxygen of the gluconate carboxylic group, other notations are as in Figs. 6-7.

Similarly to the uranyl surface complexes discussed above, the surface complexation with gluconate can also be classified as inner-sphere and outer-sphere. The inner-sphere complexes are formed when the gluconate carboxyl group is bound directly to the adsorbed cation (cation bridge, Fig. 8). The weaker outer-sphere complex is formed when solvent molecules (H_2O or OH^-) are present between the carboxyl group and the surface. Both types of complexes were observed in our simulations.

4. Conclusions

Sorption of gluconate on C-S-H phases has been studied by a combination of wet chemistry and computational molecular modelling techniques. The new results on the sorption and desorption of gluconate at very low concentrations on C-S-H were obtained. It was shown that the sorption is a rapid process and desorption is not fully reversible. The adsorption of gluconate is affected by the Ca/Si ratio of C-S-H: sorption ability of C-S-H increases for higher Ca/Si ratios showing trends similar to the ones reported in the literature (Glaus et al., 2007; Nalet and Nonat, 2016).

The molecular level structural properties of the C-S-H interfaces were investigated and local adsorption environments were identified for a range of Ca/Si ratios from 0.83 to 1.4. There are several sorption sites for uranyl cations on the C-S-H surface: monodentate and bidentate complexes can be formed with deprotonated oxygens of the surface. The same sites also adsorb Ca^{2+}, and a competition for these sites between the cations should be expected. Gluconate sorbs on the C-S-H phase by forming cation bridging inner-sphere and outer-sphere surface complexes.

The presently studied binary C-S-H-gluconate and C-S-H-uranyl systems can be considered as the first step in the comprehensive investigation of the effects of organic additives on the adsorption and mobility of radionuclides in the ternary system C-S-H-gluconate-uranyl. Quantitative evaluation of the adsorption free energies and equilibrium exchange constants for the presently identified sorption sites using the recently developed approach (Loganathan and Kalinichev, 2017) will be the focus of further studies.

Gluconate is a small organic molecule and a good starting model for the molecular scale quantitative investigation of the interaction mechanisms between organics and C-S-H surfaces. A more complex system involving polycarboxylate superplasticizer (PCE) will be also studied as the next step. This comb-shaped polymer with adsorbing anionic backbone and nonadsorbing side chains is a closer representative of a typical industrial admixture. The investigation of this more realistic system by the same experimental and computational modelling methods is currently in progress and will be reported elsewhere.

5. Acknowledgments

The study was supported by ANDRA through the PhD project of Iuliia Androniuk and through the industrial chair “Storage and Disposal of Radioactive Waste” at the Ecole des Mines de Nantes (now Institut Mines-Télécom Atlantique). Generous allocations of supercomputing resources at the CCIPL, GENCI and TGCC supercomputing facilities (projects x2014096921, x2015096921, and t2016096921) are also most gratefully acknowledged. We are also grateful to Veronique Baty (Subatech) for assistance with ion chromatography.

6. References

Allen, A.J., Thomas, J.J., Jennings, H.M., 2007. Composition and density of nanoscale calcium-silicate-hydrate in cement. Nature materials 6, 311-316.

Barret, P., Bertrandie, D., Casabonne-Masonnave, J.M., Damidot D., 1992. Short term processes of radionuclide immobilization in cement: a chemical approach. Applied Geochemistry, Suppl. 1, 109-124.

Beaudoin, J.J., Raki, L., Alizadeh, R., 2009. A 29Si MAS NMR study of modified C–S–H nanostructures. Cement & Concrete Composites 31, 585-590.

Bowers, J.M., Kirkpatrick, R.J., 2009. Natural Abundance 43Ca NMR Spectroscopy of Tobermorite and Jennite: Model Compounds for C–S–H. J. Am. Ceram. Soc. 92, 545-548.

Brunet, F., Bertani, Ph., Charpentier, Th., Nonat, A., Virlet, J., 2004. Application of 29Si Homonuclear and 1H-29Si Heteronuclear NMR Correlation to Structural Studies of Calcium Silicate Hydrates. J. Phys. Chem. B 108, 15494-15502.

Chen, J.J., Thomas, J.J., Taylor, H.F.W., Jennings, H.M., 2004. Solubility and structure of calcium silicate hydrate. Cement and Concrete Research 34, 1499-1519.

Churakov, S.V., Labbez, C., Pegado, L., Sulpizi, M., 2014. Intrinsic Acidity of Surface Sites in Calcium Silicate Hydrates and Its Implication to Their Electrokinetic Properties. J. Phys. Chem. C 118, 11752-11762.

Cong, X.D., Kirkpatrick, R.J., 1996. Si-29 MAS NMR study of the structure of calcium silicate hydrate. Advanced Cement Based Materials 3, 144-156.

Cygan, R.T., Liang, J.-J., Kalinichev, A.G., 2004. Molecular Models of Hydroxide, Oxyhydroxide, and Clay Phases and the Development of a General Force Field. J. Phys. Chem. B 108, 1255-1266.

Gaona, X., Kulik, D.A., Macé, N., Wieland, E., 2012. Aqueous–solid solution thermodynamic model of U(VI) uptake in C–S–H phases. Applied Geochemistry 27, 81-95.

Glaus, M.A., Laube, A., Van Loon, L.R., 2006. Solid–liquid distribution of selected concrete admixtures in hardened cement pastes. Waste Management 26, 741-751.

Guilbaud, P., Wipff, G., 1993. Hydration of uranyl (UO_2^{2+}) cation and its nitrate ion and 18-crown-6 adducts studied by molecular dynamics simulations. J. Phys. Chem. 97 (21), 5685–5692.

Guilbaud, P., Wipff, G., 1996. Force-field representation of the UO_2^2-energy MD simulations in water- tests on its 18-crown-6 and $NO3^-$ adducts, and on its calix[6]arene(6-) and CMPO complexes (cation from free). Journal of molecular structure. Theochem 366(1-2), 55-63.

Grambow, B., 2016. Geological disposal of radioactive waste in clay. Elements 12, 239-245.

Grangeon, S., Claret, F., Lerouge, C., Warmont, F., Sato, T., Anraku, S., Numako, C., Linard, Y., Lanson, B., 2013. On the nature if structural disorder in calcium silicate hydrate with a calcium/silicon ratio similar to tobermorite. Cement and Concrete Research 52, 31-37.

Hamid, S.A., 1981. The crystal structure of the 11Å natural tobermorite $Ca_{2.25}[Si_3O_{7.5}(OH)_{1.5}]\cdot 1H_2O$. Zeitschrift für Kristallographie 154, 189-198.

Hanehara, S., Yamada, K., 1999. Interaction between cement and chemical admixture from the point of cement hydration, absorption behaviour of admixture, and paste rheology. Cement and Concrete Research 29, 1159-1165.

Harfouche, M., Wieland, E., Daehn, R., Fujita, T., Tits, J., Kunz, D., Tsukamoto, M., 2006. EXAFS study of U(VI) uptake by calcium silicate hydrates. Journal of Colloid and Interface Science 303 (1), 195-204.

Jolicoeur, C., Simard, M.-A., 1998. Chemical Admixture-Cement Interactions: Phenomenology and Physico-Chemical Concepts. Cement and Concrete Composites 20, 87-101.

Kalinichev, A.G., Wang, J.W., Kirkpatrick, R.J., 2007. Molecular dynamics modeling of the structure, dynamics and energetics of mineral-water interfaces: Application to cement materials. Cement and Concrete Research 37, 337-347.

Kirkpatrick, R.J., Kalinichev, A.G., Hou, X., Struble, L., 2005. Experimental and molecular dynamics modeling studies of interlayer swelling: Water incorporation in kanemite and ASR gel. Materials and Structures 38, 449-458.

Ku, H.H., 1966. Notes on the Use of Propagation of Error Formulas. Journal of Research of the National Bureau of Standards - C. Engineering and Instrumentation 70C, 263-273.

Lesage, K., Vantomme, J., Cizer, O., De Schutter, G., Desmet, B., Vandewalle, L., 2014. Plasticising mechanism of sodium gluconate combined with PCE. Advances in Cement Research 27, 163-174.

Loganathan, N., Kalinichev, A.G., 2017. Quantifying the mechanisms of site-specific ion exchange at an inhomogeneously charged surface. J. Phys. Chem. C 121, in press, DOI: 10.1021/acs.jpcc.6b13108.

Lothenbach, B., Nonat, A., 2015. Calcium silicate hydrates: Solid and liquid phase composition. Cement and Concrete Research 78, 57-70.

Macé, N., Wieland, E., Dähn, R., Tits, J., Scheinost, A.C., 2013. EXAFS investigation on U(VI) immobilization in hardened cement paste: influence of experimental conditions on speciation. Radiochim. Acta 101, 379-389.

Mollah, M.Y.A., Adams, W.J., Schennach, R., Cocke, D.L., 2000. A review of cement-superplasticizer interactions and their models. Advances in Cement Research 12 (4), 153-161.

Nalet, C., Nonat, A., 2016. Ionic complexation and adsorption of small organic molecules on calcium silicate hydrate: relation with their retarding effect on the hydration of C3S. Cement and Concrete Research 89, 97-108.

Perez, J-Ph., 2007. The mechanism of action of sodium gluconate on the fluidity and set of Portland cement. Proceedings of the 12th International Congress on the Chemistry of Cement, Montreal.

Plimpton, S., 1995. Fast Parallel Algorithms for Short-Range Molecular Dynamics. J Comp Phys 117, 1-19.

Pointeau, I., Landesman, C., Giffaut, E., Reiller, P., 2004. Reproducibility of the uptake of U(VI) onto degraded cement pastes and calcium silicate hydrate phases. Radiochim. Acta 92 (9-11), 645-650.

Pointeau, I., Coreau, N., Reiller, P.E., 2008. Uptake of anionic radionuclides onto degraded cement pastes and competing effect of organic ligands. Radiochimica Acta 96 (6), 367-374.

Richardson, I.G., Skibsted, J., Black, L., Kirkpatrick, R.J., 2010. Characterisation of cement hydrate phases by TEM, NMR and Raman spectroscopy. Advances in Cement Research 22 (4), 233-248.

Sáez del Bosque, I.F., Martín-Pastor, M., Sobrados, I., Martínez-Ramírez, S., Blanco-Varela, M.T., 2016. Quantitative analysis of pure triclinic tricalcium silicate and C–S–H gels by 29Si NMR longitudinal relaxation time. Construction and Building Materials 107, 52-57.

Sanchez, F., Sobolev, K., 2010. Nanotechnology in concrete - A review. Construction and Building Materials 24, 2060-2071.

Smith, K.F., Bryan, N.D., Swinburne, A.N., Bots, P., Shaw, S., Natrajan, L.S., Mosselmans, J.F.W., Livens, F.R., Morris, K., 2015. U(VI) behaviour in hyperalkaline calcite systems. Geochimica et Cosmochimica Acta 148, 343-359.

Teich-McGoldrick, S.L., Greathouse, J.A., Cygan, R.T., 2014. Molecular dynamics simulations of uranyl adsorption and structure on the basal surface of muscovite. Molecular Simulation 40, 610-617.

Tits, J., Geipel, G., Macé, N., Eilzer, M., Wieland, E., 2011. Determination of uranium (VI) sorbed species in calcium silicate hydrate phases: a laser-induced luminescence spectroscopy and batch sorption study. J. Colloid Interf. Sci. 359, 248-256.

Tits, J., Walther., C., Stumpf, T., Macé, N., Wieland, E., 2015. A luminescence line-narrowing spectroscopic study of the uranium(VI) interaction with cementitious materials and titanium dioxide. Dalton Trans. 44, 966-976.

Viallis-Terrisse, H., Nonat, A., Petit, J.-C., 2001. Zeta-Potential Study of Calcium Silicate Hydrates Interacting with Alkaline Cations. Journal of Colloid and Interface Science 244, 58-65.

Wang, J., Wolf, R.M., Caldwell, J.W., Kollman, P.A., Case, D.A., 2004. Development and Testing of a General Amber Force Field. Journal of Computational Chemistry 25, 1157-1174.

Zhang, Z., Gibson, P., Clark, S.B., Tian, G., Zanonato, P., Rao, L., 2007. Lactonization and protonation of gluconic acid: a thermodynamic and kinetic study by potentiometry, NMR and ESI-MS. Journal of Solution Chemistry 36, 1187-1200.

Zhu, J., Li, Z., Yang, R., Zhang, Y., 2014. Organic Additive Implantation onto Cement Hydration Products. Journal of Wuhan University of Technology-Mater. Sci. Ed., 527-533.

Highlights

- Adsorption of gluconate and uranyl on calcium silicate hydrate phases (C-S-H) is studied by experimental and computational molecular modelling techniques.
- ^{14}C-labelled gluconate is used to improve the analytical sensitivity at very low concentrations (10^{-8} - 10^{-5} mol/L)
- There is a noticeably stronger gluconate sorption on C-S-H at higher Ca/Si ratios.
- Classical MD simulations help to clarify molecular mechanisms of adsorption and to identify specific surface sites most actively involved in the sorption of gluconate and uranyl on C-S-H.